Crystal structure of cytochrome P450 14α-sterol demethylase (CYP51) from *Mycobacterium tuberculosis* in complex with azole inhibitors

Larissa M. Podust*†, Thomas L. Poulos‡, and Michael R. Waterman*

*Department of Biochemistry, Vanderbilt University School of Medicine, Nashville, TN 37232-0146; and ‡Departments of Molecular Biology and Biochemistry, Physiology, and Biophysics, and the Program in Macromolecular Structure, University of California, Irvine, CA 92617-3900

Edited by Johann Deisenhofer, University of Texas Southwestern Medical Center, Dallas, TX, and approved January 17, 2001 (received for review November 26, 2000)

Cytochrome P450 14α-sterol demethylases (CYP51) are essential enzymes in sterol biosynthesis in eukaryotes. CYP51 removes the 14α-methyl group from sterol precursors such as lanosterol, obtusifoliol, dihydrolanosterol, and 24(28)-methylene-24,25-dihydrolanosterol. Inhibitors of CYP51 include triazole antifungal agents fluconazole and itraconazole, drugs used in treatment of topical and systemic mycoses. The 2.1- and 2.2-Å crystal structures reported here for 4-phenylimidazole- and fluconazole-bound CYP51 from *Mycobacterium tuberculosis* (MTCYP51) are the first structures of an authentic P450 drug target. MTCYP51 exhibits the P450 fold with the exception of two striking differences—a bent I helix and an open conformation of BC loop—that define an active site-access channel running along the heme plane perpendicular to the direction observed for the substrate entry in P450BM3. Although a channel analogous to that in P450BM3 is evident also in MTCYP51, it is not open at the surface. The presence of two different channels, with one being open to the surface, suggests the possibility of conformationally regulated substrate-in/product-out openings in CYP51. Mapping mutations identified in *Candida albicans* azole-resistant isolates indicates that azole resistance in fungi develops in protein regions involved in orchestrating passage of CYP51 through different conformational stages along the catalytic cycle rather than in residues directly contacting fluconazole. These new structures provide a basis for rational design of new, more efficacious antifungal agents as well as insight into the molecular mechanism of P450 catalysis.

Cytochrome P450 14α-sterol demethylases (CYP51s) catalyze the oxidative removal of the 14α-methyl group of lanosterol and 24-methylene-24,25-dihydrolanosterol in yeast and fungi, obtusifoliol in plants, and 24,25-dihydrolanosterol in mammals to give $\Delta^{14,15}$-desaturated intermediates in ergosterol (fungi), phytosterol (plants), and cholesterol (animals) biosynthesis. During the catalytic cycle, a substrate undergoes three successive monooxygenation reactions resulting in formation of 14-hydroxymethyl, 14-carboxaldehyde, and 14-formyl derivatives followed by elimination of formic acid with introduction of a 14,15 double bond (1, 2).

Being a key enzyme of sterol biosynthesis, CYP51 has been a target for antifungal (3) and cholesterol-lowering (4) drug design. The first generation of antifungal inhibitors of CYP51, fluconazole (FLU) and itraconazole, have revolutionized treatment of some serious fungal infections. However, the treatment of others is still far from satisfactory, and there is a need for new broad- and narrow-spectrum antifungal agents (3). Furthermore, fungal resistance caused by acquisition of intrinsically resistant species, e.g., *Aspergillus fumigatus*, or by mutation of initially susceptible strains, e.g., *Candida albicans*, is an increasing clinical problem (5, 6) forcing the development of new triazole antifungals. Azole antifungals selectively inhibit yeast and fungal CYP51 over their plant and human counterparts (7), but crossover inhibition of CYP51 in two different species can cause undesirable side effects and is another reason for the continuing search for better agents (3, 8). The problem of specificity is being addressed empirically by exploring inhibitors of different structures and by efforts to develop three-dimensional molecular models of CYP51-active sites based on primary sequence analyses and available structures for bacterial P450s. These models initially were based on the structure of P450cam (9, 10) and more recently on the structure of P450BM3 (11–14) because of its higher sequence similarity.

The available P450 structures show that the overall P450 structural fold is preserved during evolution from bacteria through mammals (15–22). At the same time, there are variable regions that appear to be associated with recognition and binding of structurally diverse substrates and redox partners (23). Experimental structural information on the active sites of the fungal, plant, and mammalian CYP51 would greatly facilitate developing more efficacious antifungal drugs. However, until recently all known forms of CYP51 were membrane-bound microsomal enzymes, which complicated structural studies of this protein by x-ray crystallography. A soluble CYP51 ortholog discovered recently in *Mycobacterium tuberculosis* (24) exhibits 35–38% sequence identity to plant, 33–35% to animal, and 26–29% to fungal enzymes. Although MTCYP51 can oxidize lanosterol and 24,25-dihydrolanosterol *in vitro*, the plant substrate obtusifoliol is preferred (25). We have crystallized *Escherichia coli*-expressed MTCYP51 in the presence of two different azole inhibitors, 4-phenylimidazole (4-PI) and FLU, and report here their structures at 2.1 and 2.2 Å, respectively.

Materials and Methods

MTCYP51 was expressed and purified as described (25). Protein of approximately 98% purity as judged by SDS gel was concentrated up to 0.2 mM in buffer containing 20 mM Tris·HCl, pH = 7.5/250 mM NaCl/0.5 mM EDTA and 4-PI at saturating concentration and subjected to crystallization. Crystals were obtained by vapor-diffusion method in a hanging drop at 22°C from 20% polyethylene glycol 4000/10% isopropanol/0.1 M Hepes, pH = 7.5 and 4-PI in saturating concentration. Crystals belong in space group $P2_12_12_1$, with unit cell dimensions a = 46.14 Å, b = 83.86 Å, c = 109.56 Å, $\alpha = \beta = \gamma = 90°$. There is one molecule per asymmetric unit. FLU was incorporated into the binding site by replacement of 4-PI in the already-formed crystal by soaking the latter in well solution containing approximately 0.5 mM FLU. Binding of FLU resulted in a small change of unit cell dimensions: a = 46.19 Å, b = 84.26 Å, c = 109.75 Å, and α =

This paper was submitted directly (Track II) to the PNAS office.

Abbreviations: 4-PI, 4-phenylimidazole; FLU, fluconazole.

Data deposition: The atomic coordinates have been deposited in the Protein Data Bank, www.rcsb.org (PDB ID codes 1E9X and 1EA1).

†To whom reprint requests should be addressed. E-mail: podustlm@ctrvax.vanderbilt.edu.

The publication costs of this article were defrayed in part by page charge payment. This article must therefore be hereby marked "*advertisement*" in accordance with 18 U.S.C. §1734 solely to indicate this fact.

www.pnas.org/cgi/doi/10.1073/pnas.061562898

Table 1. Crystallographic data

Data collection	Native	Hg	Au	FLU
Data set	4-Phenylimidazole	EMTS*	$KAu(CN)_2$	Fluconazole
Resolution, Å	2.1	2.1	2.2	2.2
Observed reflections	173,919	163,256	193,495	109,615
Unique reflections	25,107	21,756	42,188	37,242
Completeness, %	99.1 (91.3)†	91.5 (56.0)	99.4 (97.1)	95.0 (84.9)
Redundancy	6.9 (4.5)	7.5 (4.8)	4.6 (3.6)	2.9 (2.2)
$\langle I/\sigma \rangle$	9.8 (3.7)	7.1 (3.5)	7.1 (2.5)	9.7 (2.0)
R_{sym}, %‡	11.1 (48.9)	11.6 (43.3)	12.1 (47.0)	10.3 (46.5)
Phasing statistics				
Resolution range		40.0–2.8	40.0–2.8	
Sites		2	2	
Phasing power§		2.03/1.90	1.85/1.67	
R_{cullis}¶		0.46/0.62	0.46/0.66	
Quality of model				
Protein atoms	3,539			3,510
Heme atoms	43			43
Ligand atoms	11			22
Water molecules	242			175
R_{crys} (R_{free}), %‖	18.5 (23.0)			20.0 (24.9)
rms deviations				
Bonds, Å	0.005			0.007
Angles, °	1.2			1.3
Ramachandran**	89.5%			88.9%

*Ethylmercurithiosalicylic acid.
†Values in parentheses are for the highest resolution shell.
‡$R_{sym} = \Sigma \mid I_i - \langle I \rangle \mid / \Sigma \langle I \rangle$, in which $\langle I \rangle$ is the mean intensity of reflection.
§Phasing power $= \langle F_h \rangle / E$, in which $\langle F_h \rangle$ is the root mean square heavy atom structure factor and E is the residual lack of closure.
¶$R_{cullis} = \Sigma \parallel F_{ph} + F_p \mid - F_{h,c} \mid / \Sigma \mid F_{ph} + F_p \mid$, where $F_{h,c}$ is the calculated heavy atom structure factor.
‖$R_{cryst} = \Sigma \parallel F_0 \mid - \mid F_c \parallel / \Sigma \mid F_0 \mid$, calculated with the working reflection set. R_{free} is the same as R_{cryst} but calculated with the reserved reflection set.
**Program PROCHECK (36).

$\beta = \gamma = 90°$. All data were collected at the laboratory source on R-AXIS IV mounted on an RU-200 x-ray generator (Rigaku, Tokyo) at cryo temperatures. Data were processed with DENZO and scaled by using SCALEPACK (26). Data statistics are given in Table 1.

Two heavy atom derivatives were obtained by soaking 4-PI containing crystals in 1 mM solution of ethylmercurithiosalicylic acid or gold (I) potassium cyanide over several hours. Two heavy atom sites for both derivatives were localized, and the positions and occupancies were refined by using CNS (27). The molecule was traced and the model built in O (28). Native 4-PI data were used in refinement. Maximum-likelihood refinement, individual B-factors, and bulk solvent corrections were applied as implemented in CNS. The refined model was used as a search model to find molecular replacement solution for FLU-bound MTCYP51. Phasing and model quality statistics are given in Table 1.

Results and Discussion

Substrate Access Channel. MTCYP51 exhibits the P450 fold but contains striking differences that define the active site-access channel. Unlike other P450s, the longest helix in the molecule (I helix, Fig. 1) is disrupted such that the N-terminal portion bends away from the structural core making a 145° angle with the C-terminal part. Three water molecules provide H bonds to peptide groups that help compensate for missing helical H bonds. Additional stability is provided by H bonds between the side chains of T260 and Y169 and backbone peptide groups. Although comparisons of known P450 structures show nearly identical C-terminal portions of the I helix, the N-terminal halves deviate significantly from one P450 to another (Fig. 2 *A* and *B*). The MTCYP51 I helix has the most prominent N-terminal displacement, which results in bending of the I helix away from the heme that releases BC loop from closed conformation and enlarges the space available for substrate or inhibitor binding. Bending occurs at positions 253–255 in the 4-PI structure and shifts to positions 256–258 after FLU binding. The middle portion of the I helix in which the different structures start to deviate significantly from each other is well conserved among P450s, including residues A256 and G257, which tend to deviate from α-helical conformation in all known P450 structures except for P4502C5. This tendency might indicate a potential ability of the P450 I helix to bend in response to certain stimuli such as substrate or redox partner binding to release the BC loop from close contacts in the binding site. As a consequence of the large repositioning of the I helix, adjacent regions, namely the H and G helices and loops in between, also exhibit significant topological variations among P450s.

Another obvious difference is the open position of the BC loop in MTCYP51 that adopts a closed conformation in other P450 structures (Fig. 3*B*). Both the bent I helix and the open BC loop define a large opening of approximately 20 by 10 Å (Fig. 3*A*) leading from the surface of the protein to the heme. This channel (channel 1, Fig. 1) runs roughly parallel to the heme in contrast to P450BM3 and P450cam, the substrate access channel of which runs perpendicular to the heme (channel 2, Fig. 1). Channel 1 converges as an asymmetrical funnel from the surface of the protein along the heme plane. The funnel narrows to a chamber lined by residues from the B′ and I helices, β-strands β1–4 and β 4–1,2, and the loop connecting the K helix and β-strand β1–4. The chamber configuration was predicted nicely by probing of *Saccharomyces cerevisiae*-CYP51 active site with phenyldiazene (29). The dome of this active-site chamber is 10–11 Å above the

BIOCHEMISTRY

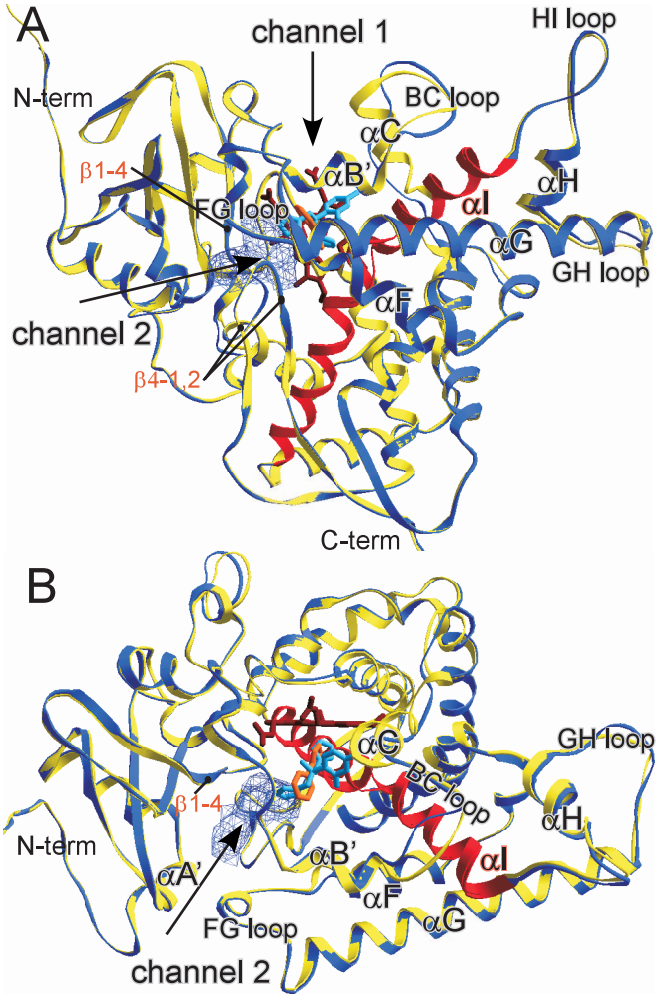

Fig. 1. Ribbon representation of the MTCYP51 structures with the inhibitors bound. Front (*A*) and top (*B*) views of the of 4-PI- (yellow) and FLU- (blue) bound MTCYP51 superimposed with an rms deviation of 0.45 Å. Superimpositions for all figures were done by using two-step fitting as implemented in SWISS-PDB VIEWER (33). The first step was performed by using entire structures; for the second step, an rms-deviation cutoff of 1.8 Å was used to select the most structurally homologous regions for subsequent fitting. The second round results in better fitting of the most homologous regions and further divergence of less homologous regions. Heme, red; 4-PI, orange; FLU, light-blue. The I helix is shown also in red. A large cavity of 2,600 Å^3, shown in blue, leads from the active site to the molecular surface along the protein domain interface (channel 2). Structural elements significantly deviating among P450 structures are labeled in black, and β-sheets that are part of the putative substrate-binding site are labeled in red. All figures, if not otherwise indicated, are generated by using SWISS-PDB VIEWER (33).

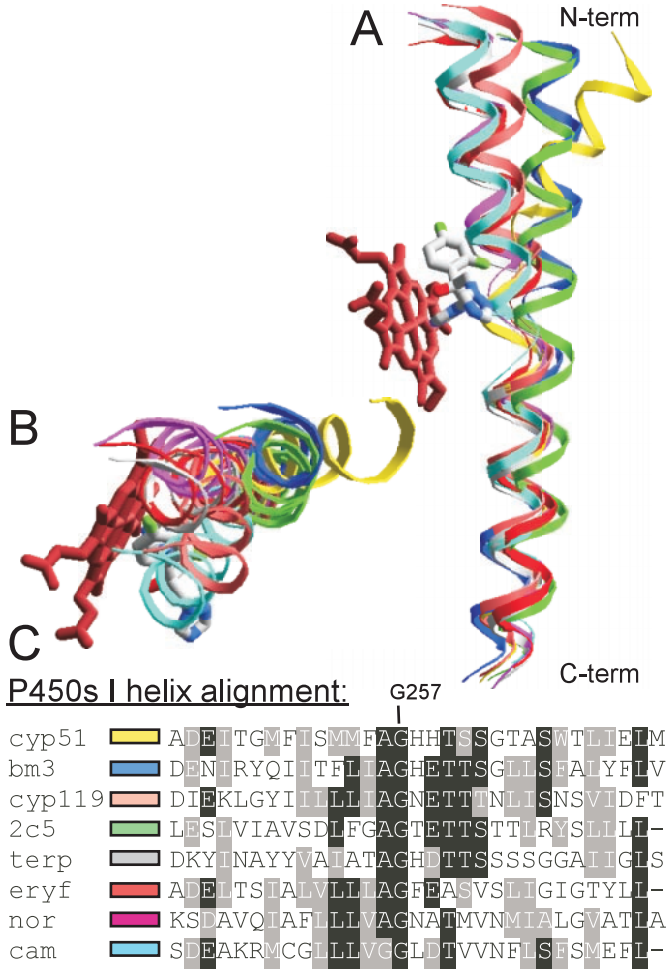

Fig. 2. Superimposition and alignment of the I helix in known P450 structures. Front (*A*) and top (*B*) views of the I helix from superimposed P450 structures assigned in sequence-alignment shown in *C*. Each structure was superimposed pairwise with MTCYP51 so that rms deviation for the most structurally homologous regions did not exceed 1.2 Å. (*C*) Alignment of the I helix sequences performed by using BCM SEARCH LAUNCHER (34). Residues identical or homologous in at least half of the compared sequences are shaded in dark or light, respectively. The position of conserved glycine is marked according to MTCYP51 sequence (P77901).

plane of the porphyrin ring. It is most open above the heme iron and pyrrole ring C with ceiling residues F78, M79, F83, and F255 (Fig. 5*A*). Access to pyrrole rings A, B, and D is limited by residues T260, A256, and L321, respectively. These side chains approach within 4 Å to the porphyrin plane.

In P450BM3, an open substrate access channel between the β-sheet and helical domains (channel 2, Fig. 1) is oriented approximately 90° relative to CYP51 channel 1 (ref. 30; Fig. 1). Although channel 2 is also apparent in the MTCYP51 structure, its entrance is closed from the surface by interaction between the A′ helix and FG loop (Fig. 1*B*). However, rotation of the F and G helices could enable an open/close motion of the FG loop as observed in P450BM3 (17, 30, 31). The movement of these two helices in P450BM3 extends through the G and H helices all of the way to the N-terminal part of the I helix (31). In MTCYP51, the loop between the H and G helices is a region with very high thermal factors (average per residue main-chain B-factor = 84.2 Å^2; Fig. 4) that enables it to accommodate a twist between these two helices. In addition, the BC loop (channel 1) followed by the C helix exhibit large main-chain thermal factors (average per residue main-chain B-factor = 58.7 Å^2. Thus, if channel 2 opens up in MTCYP51 as in P450BM3, the required structural changes would necessitate closing of channel 1. Those regions involved, the F, G, and H helices and loops in between, are known to undergo significant motion in P450BM3 when substrate binds (30, 31). This scenario provides a dynamic and synchronized picture of catalysis in which channel 1 is open, whereas channel 2 remains closed. This synchronization might provide a means for substrate to enter one channel and product to depart the other. Given the multiple oxidation steps required of CYP51, such motion may be necessary to position key residues in place for various steps along the catalytic path.

We define the BC loop as a site for "in-crystal" FLU entry on the basis of its open conformation and favorable packing mode of protein molecules in the crystal that allows sufficient open

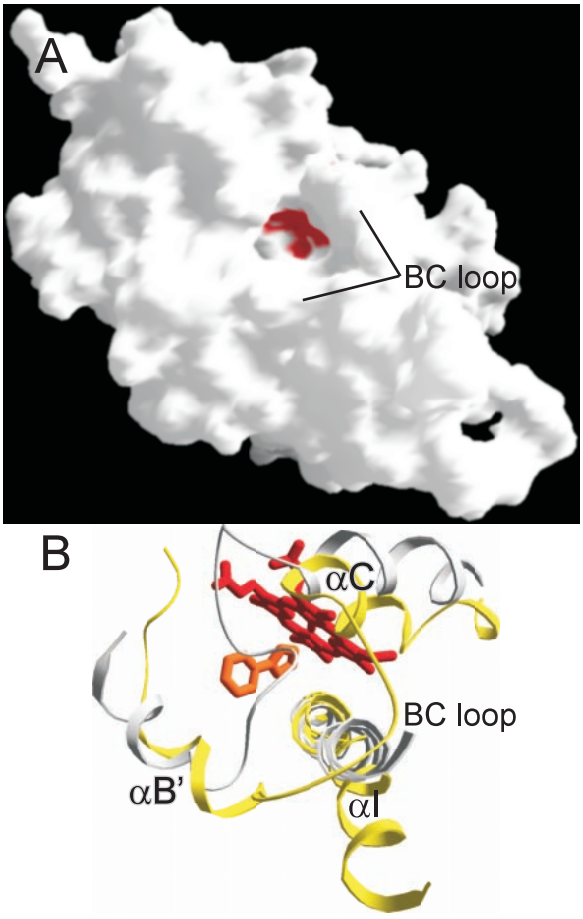

Fig. 3. (*A*) Surface representation of MTCYP51 structure. Heme, shown in red, is accessible from the surface through the open mouth of the substrate entry-channel 1. Surface was generated with GRASP (35). (*B*) View of substrate-binding site from the direction of the substrate entry along channel 1. Gray ribbon represents the P450BM3 (31), and yellow represents MTCYP51. Both structures were superimposed so that rms deviation for the most structurally homologous regions is 1.15 Å. For MTCYP51, regions of highest structural homology based on SWISS-PDB VIEWER superimposition algorithm include G41-R64, M110-C151, A256-L289, Q306-Y370, and W382-R448, which correspond to regions F40-D63, M112-C156, A264-L297, Y313-F379, and H388-K451 in P450BM3. MTCYP51 BC loop is open and lies above the N terminus of the bent I helix, which is pulled away from the structural core.

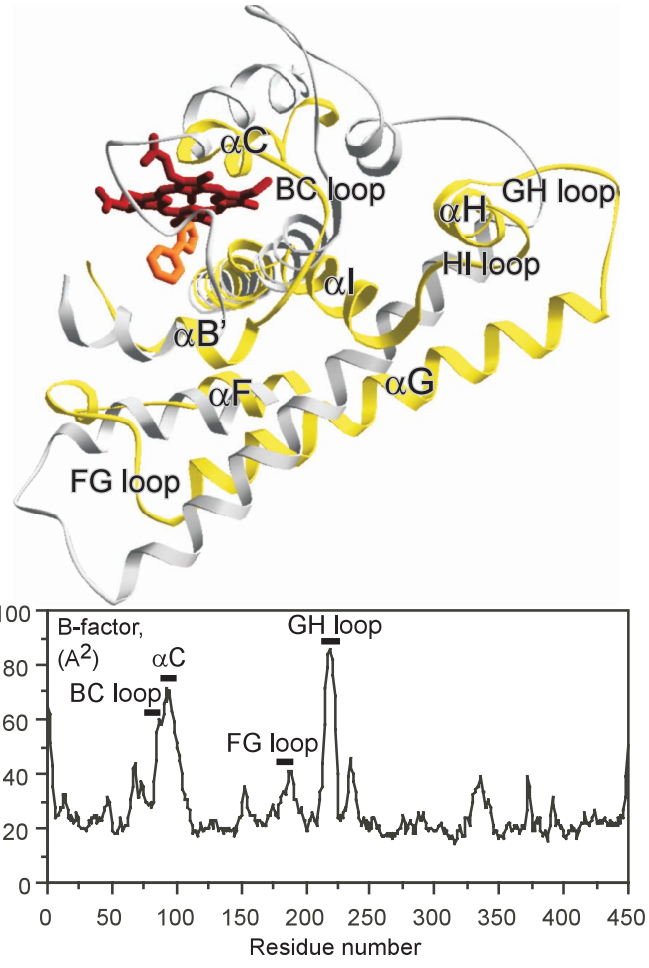

Fig. 4. Regions adjacent to the N terminus of the I helix, the H, G, and F helices, and loops in between exhibit the largest structural deviations between MTCYP51 and P450BM3 as follows from superimposition of structures described in Fig. 3. Temperature factors in MTCYP51 indicate GH and BC loops and the C helix as the most dynamic regions within the protein that could enable conformational changes required for the synchronized opening and closing of channels 1 and 2.

space for FLU to enter protein interior without damaging the crystal. The same site has been assumed to be for substrate entry in P4502C5 on the basis of increased values of thermal factors in the BC loop (21). Structural data obtained for MTCYP51 are not sufficient to determine unambiguously the direction of substrate passage *in vivo*; however, they strongly indicate the possibility that such passage might take place and would be accompanied by significant changes in protein conformation.

Inhibitor Binding. 4-PI or FLU is bound in the active site such that the imidazole ring (4-PI) or triazole ring (FLU) is positioned perpendicular to the porphyrin plane with a ring nitrogen atom coordinated to the heme iron (Fig. 5 *B* and *C*). The 4-PI phenyl group makes several nonbonded contacts with surrounding side chains, whereas the imidazole N3 H-bonds with H259. The larger size of FLU extends the number of contacts in the binding site in comparison with 4-PI. H259 is pulled away slightly from the binding site and does not form a hydrogen bond with FLU, whereas F83 and F255 provide additional nonbonded contacts. Conformational changes, which occur after binding of the larger ligand bring additional residues in close proximity to FLU. The main FLU-induced conformational changes involve a helix-coil transition of the C helix and displacement of the residues in the I helix. Region 96–100 within the disordered C helix is displaced toward the substrate-binding site (Fig. 5*C*), however the positions of side chains cannot be defined because of poor electron density for region 90–106 reflected in high values of thermal factor. The BC loop remains in an open conformation as observed in the 4-PI structure and does not close access to the substrate-binding site. However, this result cannot be considered conclusive, because 4-PI was substituted by FLU in the already-formed crystal when the motion of secondary structure elements might be restricted significantly by crystal packing interactions. Although residues H101, S252, I323, and V434 do not contact either 4-PI or FLU, they line the binding site and are likely to contribute in interaction with substrate. Active-site residues can be divided into two groups based on their conservation in different kingdoms, such as bacteria, fungi, and higher plants and animals (Table 2). Variable residues including F78, M79, K97, M99, H101, F255, S252, I323, and V434 reveal substantial differences from kingdom to kingdom, suggesting that these residues contribute to substrate specificity of CYP51 from different species.

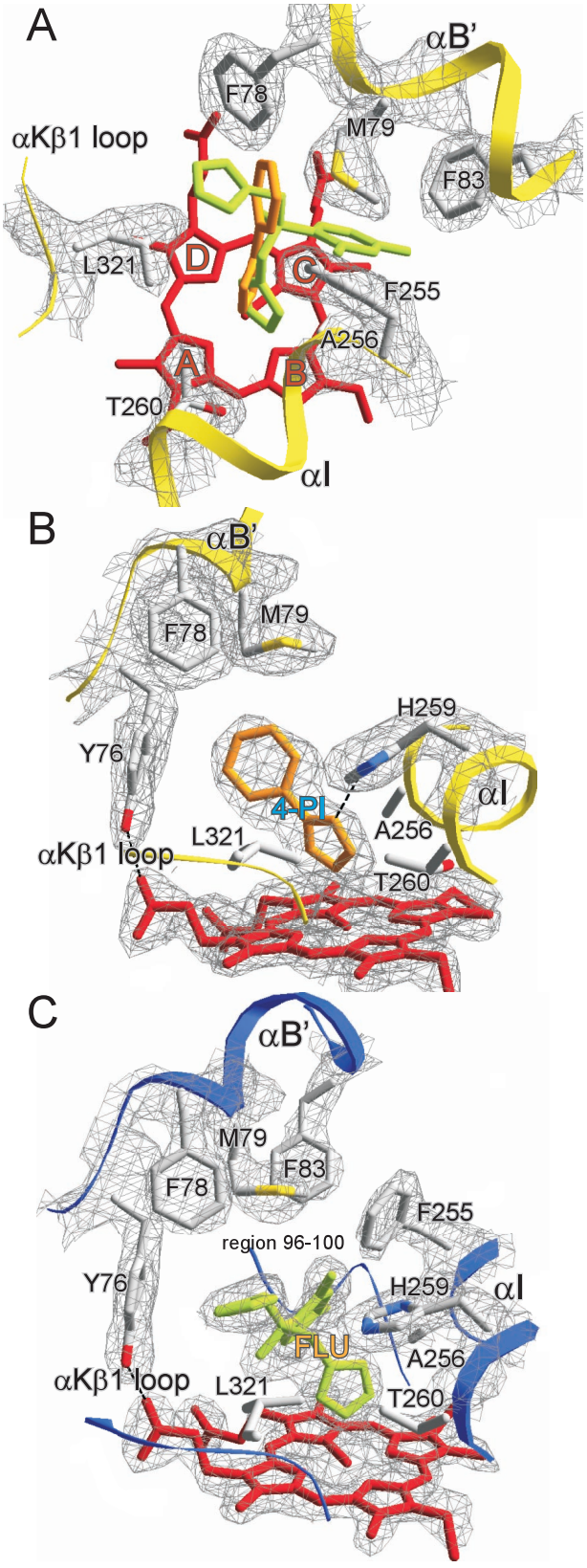

Fig. 5. (*A*) MTCYP51 active-site chamber. Structural elements and residues constituting the dome of the active site are indicated. (*B* and *C*) Interaction of 4-PI and FLU in the binding site of MTCYP51. Residues located within 4.1 Å of each ligand are shown. Region 96–100 in *C* is displaced toward the substrate-binding site as a result of conformational changes in the C helix after FLU binding. Fragments of simulated annealing omit $2F_o - F_c$ map contoured at 1.5 σ are shown.

Table 2. MTCYP51 active-site residues

MTCYP51	Plant	Mammals	Fungi
Y76	**Y**	**Y**	**Y**
F78	F	R	H(7), V(3), K(1), N(1)
M79	N	L	L
F83	**F**	**F**	**F**
F89	**F**	**Y**	**Y**
K97	Q	K	Q(11), H(1)
M99	R	M(2), I(2)	K
H101	F	—	M(4), V(3), A(3), I(2)
S252	A	G	A(6), G(5), T(1)
F255	F	L	M
H259	**H**	**H**	**H**
T260	**T**	**T**	**T(7), S(5)**
L321	**L**	**I**	**L(6), I(6)**
I323	M	T(3), I(1)	S(1), T(1)
M433	**M**	**M**	**M(7), L(4)**
V434	V	I	V(6), F(5)

Altogether, three plant, four animal, and 12 fungi CYP51 sequences were analyzed. Alignment was performed using BCM SEARCH LAUNCHER (34). Bold letters indicate residues that display significant conservation through evolution. Parentheses shows the numbers of species with indicated substitution.

Mapping of Resistant Variants. Naturally occurring CYP51 mutations identified in *C. albicans* azole-resistant isolates and clustered in three hotspots in the primary sequence (32) can be divided into four hotspots on the basis of their association with different structural regions observed in the MTCYP51 structure (Fig. 6). The first hotspot, substitutions G464S, G465S, and R467K, associates with the N-terminal part of the cysteine pocket, residues G388, A389, and G390 in MTCYP51. Positions 388 and 390 are highly conserved in P450s. These residues lie on the opposite side of the heme from where substrates bind and cannot participate directly in inhibitor binding. However, these residues provide contacts between the β-sheet and α-helical domains and may be involved in interdomain conformational changes upon inhibitor or substrate binding. Changing Gly to

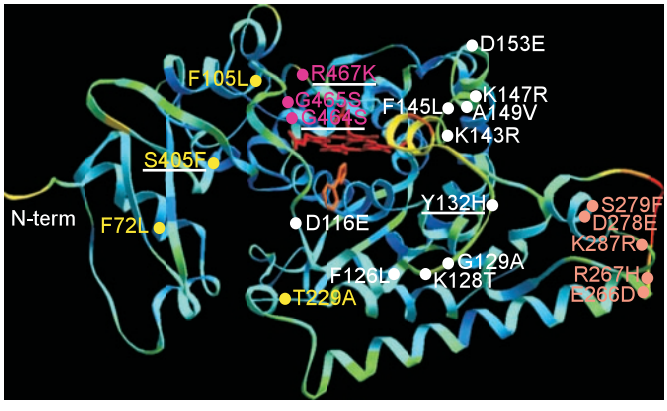

Fig. 6. Mapping of *C. albicans* mutations in azole-resistant isolates onto MTCYP51 structure. 4-PI-bound MTCYP51 is colored according to B-factor values from blue (low) to red (high). Red and yellow colors correspond to the most dynamic regions of MTCYP51. Four mutation hotspots are indicated by different colors: magenta, mutations associated with the ''cysteine pocket,'' the region of contacts between β-sheet and helical domains; rose, mutations associated with C terminus of the G helix and the H helix; yellow, mutations that associate with interdomain interface; and white, mutations that associate with the substrate entry loop. Substitutions, which have been demonstrated experimentally to be important for azole affinity, are underlined. Numbering of residues in the figure is according to *C. albicans*.

other residues would be expected to decrease flexibility required for such changes. Several other *C. albicans* mutations that we attribute to the same hotspot, including V437I, G448E, F449L, G450E, and V452A, are clustered just N-terminal to the cysteine pocket around the two glycine residues. They lack analogs in MTCYP51 structure because of the large insert occurring at this region in the fungal ortholog.

A second hotspot is mapped to the C terminus of the G helix and H helix, a region too distal to be involved in interaction with the substrate or inhibitor. Mutations here, E266D, R267H, D278E, and S279F (A214, N215, D227, and V228 in MTCYP51), flank the most dynamic residues of MTCYP51. A third hotspot, substitutions F72L, F105L, S405F, and T229A (M30, F63, S348, and D177 in MTCYP51), associates with the domain interface. Although in FLU-bound MTCYP51 these residues do not interfere with inhibitor bound in the active site, such an interaction might occur during a passage of FLU along channel 2, if such a passage exists in MTCYP51.

The fourth and final hotspot associates with the region between B′ and C helices that exhibit high thermal motion and which we have postulated is involved in inhibitor- or substrate-induced structural changes. This hotspot includes mutations D116E, F126L, K128T, G129A, Y132H, K143R, F145L, K147R, A149V, and D153E, which correspond to MTCYP51 positions K74, F83, E85, G86, F89, L100, N102, A103, A104, and E108. Being localized in the region of the mouth of channel 1, these residues could interfere with the entry of the inhibitor or its binding in the active site. Again, mutations flank the most dynamic residues rather than overlap them. The open conformation of the BC loop observed in MTCYP51 positions some of these residues, including F89 (Y132 in *C. albicans*), distant to the inhibitor. If after binding of substrate the BC loop adapts a closed conformation, these residues could come into close proximity with the active site. In P450BM3, the Phe in the corresponding position was shown to block the substrate from approaching close to the heme (31). Thus, none of the mutations identified in *C. albicans* azole-resistant isolates are involved in direct interaction with FLU when the protein is in the conformation observed in MTCYP51 crystals. Some residues from hotspots three and four, however, might encounter the inhibitor upon its passage through channel 2 or if the BC loop can adapt a closed conformation while FLU is bound in the active site. Residues in hotspots one and two lack an opportunity to interfere with FLU directly. At the same time, the regions these residues are located in are likely to be involved in conformational changes that accompany substrate binding and product release. We conclude that azole resistance in fungi develops in protein regions involved in orchestrating passage of CYP51 through the different conformational stages along the catalytic cycle. More structural and biochemical data are required to establish the proposed features of P450 catalysis and substrate and/or inhibitor binding as well as to identify a trigger to initiate protein conformational changes, although substrate binding in the active site seems a reasonable candidate.

We thank E. Howard and J. Sheehan for expert technical assistance and S. Pakhomova for assistance during data collection and many helpful discussions. L.M.P. deeply appreciates the mentoring of Dr. Youngchang Kim in the skills of x-ray crystallography. Figures were prepared by using Vanderbilt University Medical Center Cell Imaging Shared Resource supported by National Institutes of Health Grants CA68485 and DK20593. This work was supported by National Institutes of Health Grants GM37942 and ES00267 (to M.R.W.) and GM33688 (to T.L.P.).

1. Trzaskos, J., Fischer, R. & Favata, M. (1986) *J. Biol. Chem.* **261,** 16937–16942.
2. Aoyama, Y., Yoshida, Y., Sonoda, Y. & Sato, Y. (1989) *J. Biol. Chem.* **264,** 18502–18505.
3. Sheehan, D. J., Hitchcoch, C. A. & Sibley, C. M. (1999) *Clin. Microbiol. Rev.* **12,** 40–79.
4. Frye, L. L. & Leonard, D. A. (1999) *Crit. Rev. Biochem. Mol. Biol.* **34,** 123–140.
5. Koltin, Y. & Hitchcock, C. A. (1997) *Curr. Opin. Chem. Biol.* **1,** 176–182.
6. Vanden Bossche, H., Dromer, F., Improvisi, I., Lozano-Chiu, M., Rex, J. H. & Sanglard, D. (1998) *Med. Mycol.* **36,** Suppl. 1, 119–128.
7. Georgopapadakou, N. H. (1998) *Curr. Opin. Microbiol.* **1,** 547–557.
8. DiDomenico, B. (1999) *Curr. Opin. Microbiol.* **2,** 509–515.
9. Morris, G. M. & Richards, W. G. (1991) *Biochem. Soc. Trans.* **19,** 793–795.
10. Boscott, P. E. & Grant, G. H. (1994) *J. Mol. Graphics* **12,** 185–192.
11. Holtje, H.-D. & Fattorusso, C. (1998) *Pharm. Acta Helv.* **72,** 271–277.
12. Tsukuda, T., Shiratori, Y., Watanabe, M., Ontsuka, H., Hattori, K., Shirai, M. & Shimma, N. (1998) *Bioorg. Med. Chem. Lett.* **8,** 1819–1824.
13. Lewis, D. F. V., Wiseman, A. & Tarbit, M. H. (1999) *J. Enzyme Inhib.* **14,** 175–192.
14. Ji, H., Zhang, W., Zhou, Y., Zhang, M., Zhu, J., Song, Y. & Lu, J. (2000) *J. Med. Chem.* **43,** 2493–2505.
15. Poulos, T. L., Finzel, B. C., Gunsalus, I. C., Wagner, G. C. & Kraut, J. (1985) *J. Biol. Chem.* **260,** 16122–16130.
16. Poulos, T. L., Finzel, B. C. & Howard, A. J. (1987) *J. Mol. Biol.* **195,** 687–700.
17. Ravichandran, K. G., Boddupalli, S. S., Hasemann, C. A., Peterson, J. A. & Deisenhofer, J. (1993) *Science* **261,** 731–736.
18. Hasemann, C. A., Ravichandran, K. G., Peterson, J. A. & Deisenhofer, J. (1994) *J. Mol. Biol.* **236,** 1169–1185.
19. Cupp-Vickery, J. R. & Poulos, T. L. (1995) *Nat. Struct. Biol.* **2,** 144–153.
20. Park, S. Y., Shimizu, H., Adachi, S., Nakagava, A., Tanaka, I., Nakahara, K., Shoun, H., Obayashi, E., Nakamura, H., Iizuka, T. & Shiro, Y. (1997) *Nat. Struct. Biol.* **4,** 827–832.
21. Williams, P. A., Cosme, J., Sridhar, V., Johnson, E. F. & McRee, D. E. (2000) *Mol. Cell* **5,** 121–131.
22. Yano, J. K., Koo, L. S., Schuller, D. J., Li, H., Ortiz de Montellano, P. R. & Poulos, T. L. (2000) *J. Biol. Chem.* **275,** 31086–31092.
23. Graham, S. E. & Peterson, J. A. (1999) *Arch. Biochem. Biophys.* **369,** 24–29.
24. Aoyama, Y., Horiuchi, T., Gotoh, O., Noshiro, M. & Yoshida, Y. (1998) *J. Biochem (Tokyo)* **124,** 694–696.
25. Bellamine, A., Mangla, A. T., Nes, W. D. & Waterman, M. R. (1999) *Proc. Natl. Acad. Sci. USA* **96,** 8937–8942.
26. Otwinowski, Z. & Minor, W. (1997) *Methods Enzymol.* **276,** 307–326.
27. Brunger, A. T., Adams, P. D., Clore, G. M., Delano, W. L., Gros, P., Grosse-Kunstleve, R. W., Jiang, J.-S., Kuszewski, J., Nilges, M. & Pannu, N. S. (1998) *Acta Crystallogr. D* **54,** 905–921.
28. Jones, T. A., Zou, J. Y., Cowan, S. W. & Kjeldgaard, M. (1991) *Acta Crysallogr. A* **47,** 110–119.
29. Tuck, S. F., Aoyama, Y., Yoshida, Y. & Ortiz de Montellano, P. R. (1992) *J. Biol. Chem.* **267,** 13175–13179.
30. Li, H. & Poulos, T. L. (1996) *Biochimie* **78,** 695–699.
31. Li, H. & Poulos, T. L. (1997) *Nat. Struct. Biol.* **4,** 140–146.
32. Marichal, P., Koymans, L., Willemsens, S., Bellens, D., Verhasselt, P., Luyten, W., Borgers, M., Ramaekers, F. C. S., Odds, F. C. & Bossche, H. V. (1999) *Microbiology* **145,** 2701–2713.
33. Guex, N. & Peitsch, M. C. (1997) *Electrophoresis* **18,** 2714–2723.
34. Smith, R. F., Wiese, B. A., Wojzynski, M. K., Davison, D. B. & Worley, K. C. (1996) *Genome Res.* **6,** 454–462.
35. Nicholls, A., Sharp, K. A. & Honig, B. (1991) *Proteins* **11,** 281–296.
36. Laskowski, R. A., MacArthur, M. W., Moss, D. S. & Thornton, J. M. (1993) *J. Appl. Crystallogr.* **26,** 283–291.